Nonstationarity in Intermittent Rainfall: The "Dry Drift"

MARC SCHLEISS,* SABINE CHAMOUN,+ AND ALEXIS BERNE

Laboratoire de Télédétection Environnementale, École Polytechnique Fédérale de Lausanne, Lausanne, Switzerland

(Manuscript received 24 May 2013, in final form 15 January 2014)

ABSTRACT

A particular aspect of the nonstationary nature of intermittent rainfall is investigated. It manifests itself in the fact that the average rain rate varies with the distance to the surrounding dry areas. The authors call this fundamental link between the rainfall intensity and the rainfall occurrence process the "dry drift." Using high-resolution radar rain-rate maps and disdrometer data, they show how the dry drift affects the structure and the variability of intermittent rainfall fields. They provide a rigorous geostatistical framework to describe it and propose an extension of the concept to more general quantities like the (rain)drop size distribution.

1. Introduction

Space–time variability of rainfall is an important source of uncertainty that must be properly taken into account. A distinctive feature of rainfall variability at the meso-gamma and mesobeta scales (i.e., from 1 to 200 km) is intermittency (Kundu and Siddani 2011; Schleiss et al. 2011). Intermittency limits the available water resources in time and space and directly affects the environment and the ecosystems (e.g., Porporato and Rodriguez-Iturbe 2004; Mandapaka et al. 2009).

A variety of approaches have been proposed to deal with intermittency in rainfall models. Using a multifractal framework, Over and Gupta (1994) suggested to represent dry and rainy regions using a special random cascade known as a β model. Albeit useful, the β model turned out to be too simplistic to fully describe the distribution and the space–time structure of rainfall intermittency (Schmitt et al. 1998). Since then, and despite several decades of research and numerous alternatives (e.g., Olsson 1998; Schmitt et al. 1998; de Montera et al. 2009; Gires et al. 2013), the correct representation of intermittency within the multifractal framework still remains an open question.

In the geostatistical framework proposed by Barancourt et al. (1992), intermittency is represented by a rainfall occurrence process $I_R \in \{0, 1\}$, defined as

$$I_R(\mathbf{x}, t) = \begin{cases} 1 & \text{if} \quad R(\mathbf{x}, t) > 0 \\ 0 & \text{if} \quad R(\mathbf{x}, t) = 0 \end{cases}, \tag{1}$$

where $R(\mathbf{x}, t)$ (mm h^{-1}) represents the instantaneous rain rate at location $\mathbf{x} \in \mathbb{R}^2$ and time $t \in \mathbb{R}$. The approach is very popular and widely used in practical applications involving rainfall interpolation, simulation, and disaggregation (e.g., Kumar and Foufoula-Georgiou 1993; Syed et al. 2003; De Oliveira 2004; Berrocal et al. 2008).

To model their structure using variograms, I_R and R are usually assumed to be second-order or intrinsically stationary. In particular, the expected rain rate $\mathbb{E}[R(\mathbf{x}, t)]$ at location $\mathbf{x}$ and time t is assumed to be constant or linear in $\mathbf{x}$ and t. Proving or refuting second-order (or intrinsic) stationarity is a very difficult problem in general, especially for cases where there is only a single available realization. The key problem with stationarity, however, is that it leads to a counterintuitive representation of rainfall in which the average rain rate is independent from the occurrence process. In particular, it contradicts the fact that rain rates may decrease when approaching a dry area/period (e.g., Emmanuel et al. 2012). Interestingly, Barancourt et al. (1992) devote a full section to this problem, analyzing what they call the

* Current affiliation: Civil and Environmental Engineering, Princeton University, Princeton, New Jersey.

+ Current affiliation: Hydraulics Constructions Laboratory, École Polytechnique Fédérale de Lausanne, Lausanne, Switzerland.

Corresponding author address: Alexis Berne, Laboratoire de Télédétection Environnementale, EPFL, Station 2, Lausanne 1015, Switzerland.
E-mail: alexis.berne@epfl.ch

DOI: 10.1175/JHM-D-13-095.1

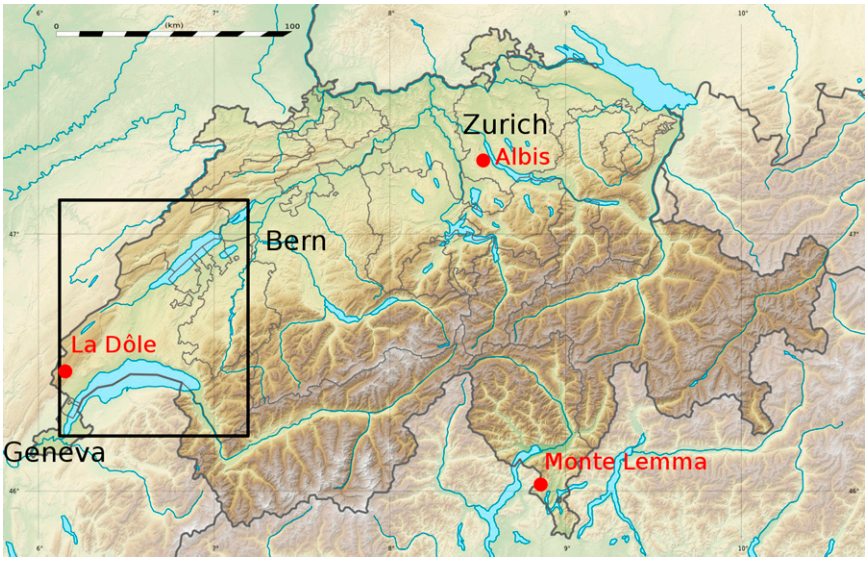

FIG. 1. Topographic map of Switzerland with the selected area of study (black rectangle) and the location of the 3 C-band MeteoSwiss weather radars (red dots).

"inner drift." They conclude, however, that the inner drift is "moderate" (for the considered dataset) and that I_R and R can be assumed independent. This is a strong assumption that is not supported by the results presented in this study.

Following a similar approach, Braud et al. (1994) analyzed the spatial distribution of rain-rate values inside τ-thresholded rainy areas (i.e., areas with rain rates larger than a given threshold τ). Their study showed that the average rain rate (at time t) at a given location $\mathbf{x}$ inside a τ-thresholded rainy area $A(\tau, t)$ depends on the distance $d(\mathbf{x})$ from $\mathbf{x}$ to the boundary of $A(\tau, t)$. This dependency is represented using so-called internal moving trend functions (MTFs) and approximated using a spherical function. In their study, Braud et al. (1994) present MTFs as a useful tool for estimating mean areal rain rates but do not investigate how these trends affect the spatial structure (i.e., the sample variogram) of a rainfall field.

In this article, we revisit the concept of moving trend functions proposed by Braud et al. (1994) for the special case $\tau = 0$, that is, the case where the average rain rate is a function of the distance to the closest dry area (hereinafter referred to as the "dry drift"). We provide a new and rigorous geostatistical framework for this concept and show why it is more appropriate to define it for log-transformed rain rates rather than in the linear space. Possible extensions of the concept to other quantities like the (rain)drop size distribution (DSD) are also proposed. The results show that dry drifts constitute an important (yet not the only) source of nonstationarity and that they significantly affect the structure and the space–time variability of rainfall.

This article is structured as follows. Section 2 describes the data used for the analysis. Section 3 introduces the concept of dry drift for two-dimensional rain-rate fields and discusses some of its characteristics. Section 4 describes the equivalents for time series and space–time data and extends the concept to more general quantities. In section 5, we highlight the importance of dry drifts for structural analysis, remote sensing, and stochastic rainfall simulation by providing different examples of applications. Section 6 summarizes the main ideas and provides some perspectives for future work.

2. Data

The results presented in this paper are based on the analysis of radar rain-rate maps and disdrometer time series. A brief description of these data is given below.

a. Radar rain-rate maps

The data used for the spatial analysis of intermittent rainfall fields were provided by the Swiss Federal Office of Meteorology (MeteoSwiss). They consist of Cartesian radar rain-rate maps with a spatial resolution of $1 \times 1\,\text{km}^2$ and a temporal resolution of 5 min (2.5 min since 2012). Each map was obtained by combining the measurements of 3 C-band weather radars scanning at various elevations, correcting for the main sources of errors (ground clutter, beam shielding, and vertical variability) according to a procedure described in Germann et al. (2006). To ensure that the data were reliable, the analysis was restricted to a small area of size $80 \times 100\,\text{km}^2$ in the northeast of Geneva (Fig. 1), for which the data are

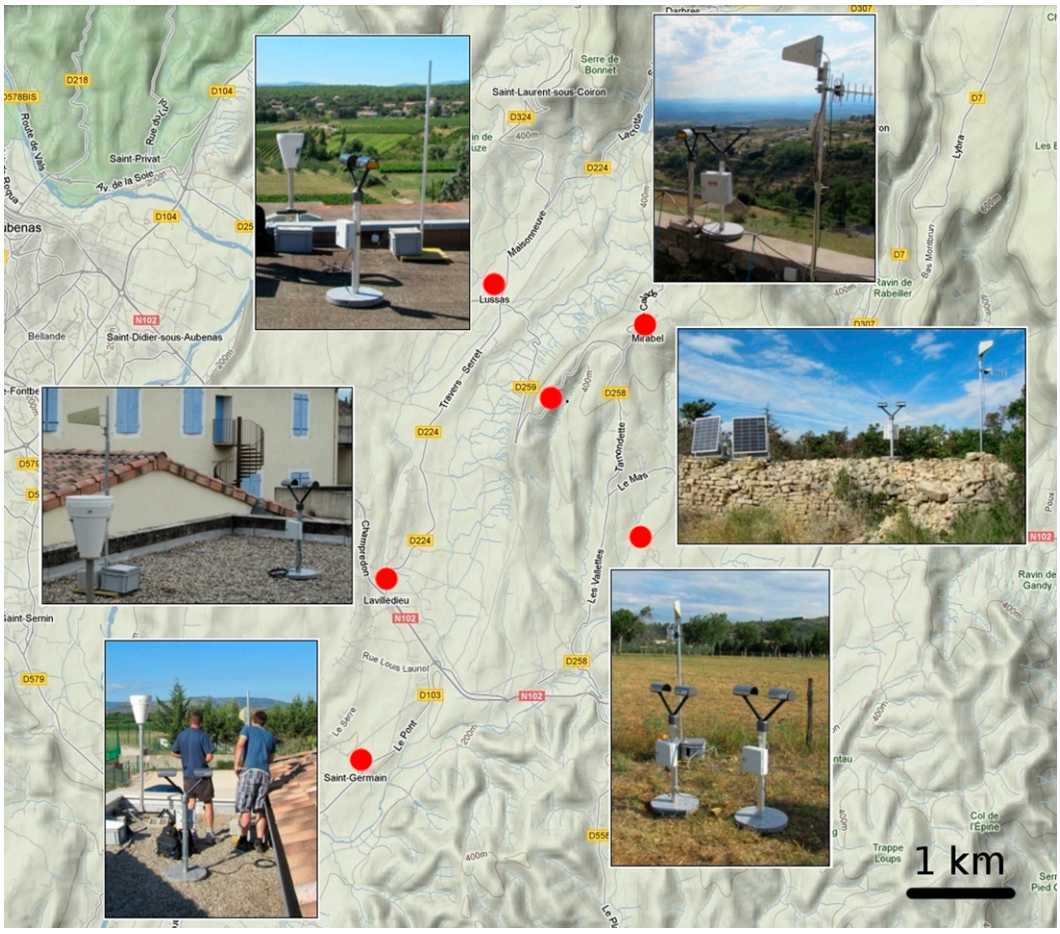

FIG. 2. Location and illustration of the seven optical disdrometers (red dots) deployed during the HyMeX in Ardèche, France.

believed to be of good quality. The rain/no-rain information needed to define the rainfall occurrence process was directly retrieved from the rain-rate maps. Because it is relatively easy to distinguish between dry and rainy regions using weather radar, the false dry and rain detection rates over the considered area are assumed to be negligible.

b. Disdrometer time series

To analyze the temporal variability of intermittent rainfall (including the raindrop size distribution and associated bulk variables), data from seven optical disdrometers of type Parsivel (Löffler-Mang and Joss 2000) were used. These disdrometers were part of the Hydrological Cycle in Mediterranean Experiment (HyMeX; www.hymex.org) and were deployed at six different locations in Ardèche, France (Fig. 2). Each disdrometer collected DSD time series at the point scale with a temporal resolution of 30 s. All DSD spectra were processed, filtered, and quality controlled following a procedure proposed by Jaffrain et al. (2011). All solid and mixed-phased precipitation types, as well as other nonmeteorological signals (e.g., spiders and insects), were removed. The rain amounts derived from the DSD time series were in excellent agreement with nearby tipping rain gauges (bias of less than 10%).

3. Spatial dry drifts

This section is devoted to the description of the dry drift. For conciseness, the concept will only be described in detail for two-dimensional rain-rate fields. For the one-dimensional counterpart, the complete space–time formulation and extensions to other DSD-related quantities, the reader is referred to section 4.

Following the approach proposed by Barancourt et al. (1992), we separate the dry regions from the rainy ones and focus on strictly positive rain-rate values ($R > 0$). Because positive rain-rate values have a skewed distribution, close to a lognormal, it is preferable

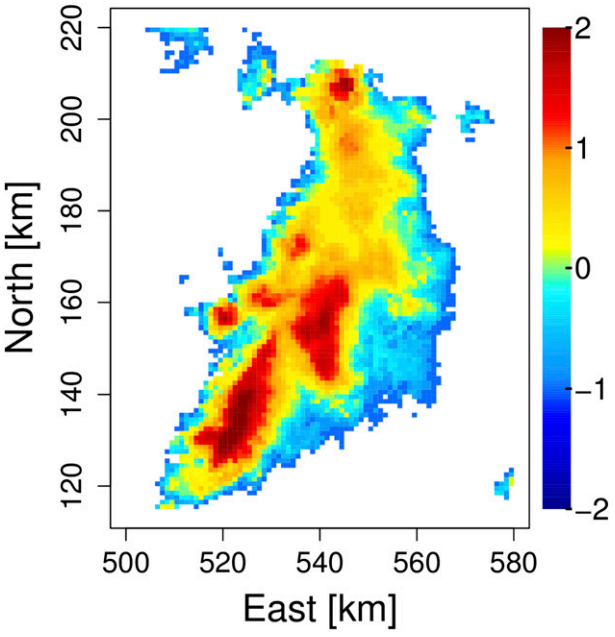

FIG. 3. Best radar estimation of the log-transformed rain rate (mm h^{-1}) at the ground level for a convective storm on 1 Aug 2012 at 1915 UTC. Dry regions are represented in white. For more details on this product, see section 2a.

to work with the log-transformed rain-rate values (Journel 1980):

$$\tilde{R}(\mathbf{x}) = \log_{10}[R(\mathbf{x})]. \tag{2}$$

Log-transformed rain-rate values have a more symmetrical distribution (i.e., closer to a Gaussian distribution) and are therefore better suited for structural analysis. Working in the log space also makes it easier to add/remove possible trends without having to threshold negative rain-rate values. In addition to these two advantages, the log transform also helps in "stabilizing" the variance of the rain-rate field (see section 3b). An example of a log-transformed radar rain-rate map is given in Fig. 3.

a. The dry drift function

For consistency, we assume that the log-transformed rain-rate field $\tilde{R}$ can be seen as a random function in space and that its (unknown) expectation $m_{\tilde{R}}(\mathbf{x}) = \mathbb{E}[\tilde{R}(\mathbf{x})]$ is well-defined at each rainy location $\mathbf{x}$. Consequently, the rainfall intensity process can be decomposed and represented as the sum of a deterministic trend function $m_{\tilde{R}}$ and a stochastic component $R^{\star}$, defined as

$$\tilde{R}(\mathbf{x}) = m_{\tilde{R}}(\mathbf{x}) + R^{\star}(\mathbf{x}), \tag{3}$$

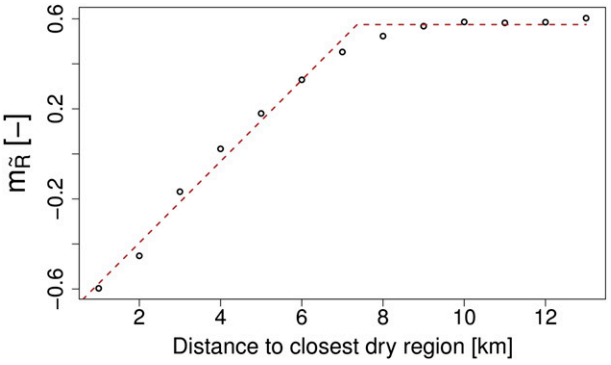

FIG. 4. Estimated isotropic spatial dry drift corresponding to the rain-rate map shown in Fig. 3. The dashed red line represents the fitted piecewise linear dry drift model given in Eq. (8). The class width is 1 km.

where $\mathbb{E}[R^{\star}(\mathbf{x})] = 0$ for all $\mathbf{x}$. In other words, there is a function $m_{\tilde{R}}$ that represents the general rain-rate trend over the domain and a centered residual stochastic process $R^{\star}$ that describes random structured variations around this trend. The major challenge in this procedure is to find an adequate model for $m_{\tilde{R}}$ (using only a single realization of R). Because this is very difficult in general, it is often assumed that $\tilde{R}$ is second-order stationary and that $m_{\tilde{R}}$ is constant over the entire domain.

The approach proposed in this article is different: instead of analyzing the rain-rate process with respect to its spatial coordinates, we start by projecting it onto a smaller, one-dimensional distance space. This distance space is generated by the rainfall occurrence process I_R and the Euclidean distance $d(\mathbf{x})$ between a rainy location $\mathbf{x}$ and the closest surrounding dry region in the domain:

$$d : \{\mathbf{x} \in \mathbb{R}^2 \mid I_R(\mathbf{x}) = 1\} \mapsto \mathbb{R}^+, \tag{4}$$

$$d(\mathbf{x}) = \min_{\mathbf{y} \in \Omega} \{\|\mathbf{x} - \mathbf{y}\|\}, \quad \text{and} \tag{5}$$

$$\Omega = \{\mathbf{y} \in \mathbb{R}^2 \mid I_R(\mathbf{y}) = 0\}, \tag{6}$$

where $\{\cdot\}$ indicates a set and $\|\cdot\|$ represents the Euclidean norm in $\mathbb{R}^2$. The motivation behind this approach is the assumption that the expected rain rate $m_{\tilde{R}}(\mathbf{x})$ is easier to describe as a function of $d(\mathbf{x})$ rather than $\mathbf{x}$:

$$m_{\tilde{R}}(\mathbf{x}) = f[d(\mathbf{x})], \tag{7}$$

where f: $\mathbb{R}^+ \mapsto \mathbb{R}$ is called the dry drift. Using high-resolution radar data, it is possible to estimate and parameterize the function f for different events and different types of precipitation (see section 3c for more details).

Figure 4 illustrates the typical characteristics of a dry drift function: the drift is minimum at $d = 0$ and

increases with d until it reaches a maximum value $M = f(d_M)$. For larger distances, the expected rain-rate value stays relatively constant. In other words, there is a distance d_M (7.5 km in this particular case) after which the effect of the dry regions on the average rain rate can be neglected. We call this distance the ''maximum distance of influence.'' Based on the analysis of 14 stratiform and 14 convective rain events of various duration between 2009 and 2011, the authors found that most dry drifts (for log-transformed rain rates) exhibit a similar behavior and can be modeled using a piecewise linear function of d:

$$f(d) = \begin{cases} m_0 + m_1 d & \text{if} \quad d \le d_M \\ M & \text{else} \end{cases} \quad \text{and} \tag{8}$$

$$d_M = \frac{M - m_0}{m_1}, \tag{9}$$

where the intercept $m_0 \in \mathbb{R}$ (nondimensional), the slope $m_1 > 0$ (km^{-1}), and the magnitude $M > m_0$ (nondimensional) of the dry drift depend on the selected event and the rainfall type. It is important to point out that the linear dry drift model proposed above only provides the best fit on average (for all the considered events). Other functional forms (e.g., a spherical or an exponential function) may also be considered depending on the considered case.

b. The detrended rain rate

Note that the dry drift is a rather peculiar and unusual trend. It is defined with respect to the rainfall occurrence field (which is a stochastic process), and is therefore, strictly speaking, itself a random field. Conditionally on the occurrence process, the dry drift is, however, fully deterministic. Once it is known, it can be removed to produce the detrended rain-rate field $R^\star$:

$$R^\star(\mathbf{x}) = \tilde{R}(\mathbf{x}) - f[d(\mathbf{x})]. \tag{10}$$

By definition, $R^\star$ captures all random variations of $\tilde{R}$ around the dry drift. Its expectation is constant and equal to zero at any location in the domain. Its variance (and higher-order moments) may, however, still depend on the distance d to the closest dry region. To address this issue, the authors computed the 10%, 25%, 50%, 75%, and 90% quantiles of $\tilde{R}$ for each distance class d. The latter are shown in the form of box plots in the top panel of Fig. 5. For comparison, the bottom panel shows the same quantiles but without the initial log transform. One can see that the variability of R strongly varies with d. The log transform reduces this heteroscedasticity and helps to stabilize the variance (and higher-order moments) of $\tilde{R}$. Additional analyses for different events confirm this ''variance stabilization'' property of the log transform. In view of these results, the authors chose to neglect higher-order dry drifts (i.e., drifts in variances and higher-order moments).

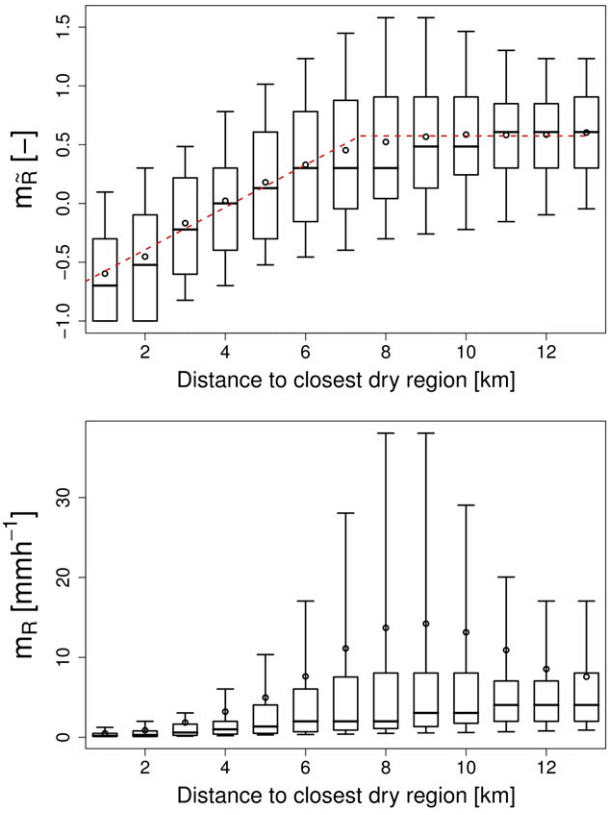

FIG. 5. Estimated isotropic spatial dry drift (black dots) in (top) the log space and (bottom) the linear space for the radar rain-rate map shown in Fig. 3. The box plots represent the 10%, 25%, 50%, 75%, and 90% quantiles for each class of distance. The dashed red line represents the fitted dry drift model shown in Fig. 4. The class width is 1 km.

c. Sample estimate of the isotropic dry drift

In the following, we briefly describe how the dry drift can be estimated from a given sample rain-rate field. For simplicity, only radar rain-rate maps will be considered. Other cases (e.g., rain gauge networks) for which the distance $d(\mathbf{x})$ to the closest dry area is more difficult to determine (depending on the density of the network) will not be addressed. Note also that because dry drifts can extend over several kilometers in space, the sampling domain must be sufficiently large. As a rule of thumb, the domain size should not be smaller than $30 \times 30\,\text{km}^2$ and should contain at least 15–20 dry pixels and 200–300 rainy pixels (preferably at various distances from the dry areas).

TABLE 1. The 2.5% quantile (q2.5), mean, and 97.5% quantile (q97.5) of m_0, m_1, M, and d_M for 14 stratiform and 14 convective events in Switzerland during 2009 and 2011. The dry drift model was fitted every 5 min (e.g., there are 12 different values of m_0, m_1, M, and d_M for each hour of rainfall).

	Stratiform			Convective		
Parameter	q2.5	Mean	q97.5	q2.5	Mean	q97.5
m_0 (-)	−1.78	−1.33	−0.80	−1.74	−1.14	−0.26
m_1 (km^{-1})	0.03	0.21	0.57	0.08	0.38	0.99
M (-)	−1.04	−0.19	0.97	−0.56	0.91	2.90
d_M (km)	3.1	5.4	24.7	3.2	5.4	14.8

For radar rain-rate maps, the dry drift $f(d)$ for a given distance d can be estimated using the following estimate:

$$\hat{f}(d) = \frac{1}{n_d} \sum_{\mathbf{x}_i \in S_d} \tilde{R}(\mathbf{x}_i) \quad \text{and} \tag{11}$$

$$S_d = \{\mathbf{x}_i \,|\, I_R(\mathbf{x}_i) = 1 \quad \text{and} \quad |d(\mathbf{x}_i) - d| \le \varepsilon\}, \tag{12}$$

where n_d denotes the number of elements in S_d and $\varepsilon > 0$ is a small tolerance on the distance to the closest dry area. The assumption behind Eq. (11) is that, for each distance d, $\tilde{R}$ restricted to $\{\mathbf{x} \in \mathbb{R}^2 \,|\, d(\mathbf{x}) = d\}$ is an ergodic random function.

Note that to estimate the dry drift, one must be able to correctly determine the distance $d(\mathbf{x}_i)$ from any rainy location $\mathbf{x}_i$ to the closest surrounding dry region. For most pixels, this is straightforward because the closest dry region lies inside the domain of interest. For pixels closer to the border, however, there is always a risk that the closest dry region may be located outside the considered domain. To avoid biased dry drift estimates, it is necessary to identify and to remove all these pixels. More specifically, one must remove all rainy pixels for which the distance to the border is smaller than the distance to the closest dry pixel in the domain.

Using the piecewise linear dry drift model in Eq. (8) and the dry drift estimation method provided above, the authors computed and fitted the dry drift parameters m_0, m_1, M, and d_M (using least squares) for each time step of the 14 stratiform and 14 convective rain events between 2009 and 2011. The average estimated values of m_0, m_1, M, and d_M for each precipitation type are given in Table 1. Comparing the values in Table 1, one can see that the maximum distance of influence d_M (5.4 km on average) is almost identical during stratiform and convective events. The intercept m_0 and the slope m_1, on the other hand, slightly depend on the rainfall type. The parameter that depends the most on the type of rainfall is clearly the magnitude M of the dry drift. It is larger during convective events and significantly varies from one event to another.

If, for any reason, the dry drift cannot be estimated properly from the sample (e.g., because there are not enough sample values per distance class to reliably estimate the average rain rate), then the average values of m_0, m_1, M, and d_M provided in Table 1 can be used as a climatological parameterization for the dry drift. A slightly better approach is to use the climatological values of m_0 and d_M and to estimate the values of M and m_1 for the considered sample:

$$\hat{M} = \frac{1}{n^{\star}_{d_M}} \sum_{\mathbf{x}_i \in S^{\star}_{d_M}} \tilde{R}(\mathbf{x}_i), \tag{13}$$

$$\widehat{m_1} = \frac{\hat{M} - m_0}{d_M}, \quad \text{and} \tag{14}$$

$$S^{\star}_{d_M} = \{\mathbf{x}_i \,|\, I_R(\mathbf{x}_i) = 1 \quad \text{and} \quad d(\mathbf{x}_i) \ge d_M\}, \tag{15}$$

where $n^{\star}_{d_M}$ represents the number of elements in the set $S^{\star}_{d_M}$. This has the advantage of providing dry drift functions for which the magnitude M of the dry drift (i.e., the average rain rate far from the dry regions) is consistent with the average rain rate in the sample.

d. Spatial anisotropy

Like variograms, dry drifts can be either isotropic or anisotropic. In the isotropic case, the average rain rate solely depends on the Euclidean distance $d(\mathbf{x})$ from $\mathbf{x}$ to the nearest dry region. In the anisotropic case, the average rain rate depends both on the distance and on the direction to the nearest dry region:

$$m_{\tilde{R}}(\mathbf{x}) = g[\mathbf{h}(\mathbf{x})], \tag{16}$$

where $g: \mathbb{R}^2 \mapsto \mathbb{R}$ is the anisotropic dry drift function and $\mathbf{h}(\mathbf{x}) \in \mathbb{R}^2$ represents the vector from $\mathbf{x}$ to the nearest dry region in the domain. If the dry drift is isotropic, we have $g[\mathbf{h}(\mathbf{x})] = f[\|\mathbf{h}(\mathbf{x})\|] \; \forall \; \mathbf{h}(\mathbf{x}) \in \mathbb{R}^2$. For a visual illustration of an anisotropic dry drift, see Fig. 6. It is worth mentioning that, unlike variograms, dry drifts are not necessarily symmetric (as shown in Fig. 6). It can therefore be difficult to find good and simple mathematical models to represent them. In general, and unless there is clear evidence suggesting otherwise, the simpler isotropic dry drift model should be preferred over the anisotropic one because it has fewer parameters and can be estimated more easily from the data. Its parameters are also easier to interpret. There are, however, some special cases where the use of a more complicated anisotropic dry drift may be justified. Squall lines and frontal systems, for example, are characterized by strong rain-rate gradients at the front and much weaker gradients on the other side of the

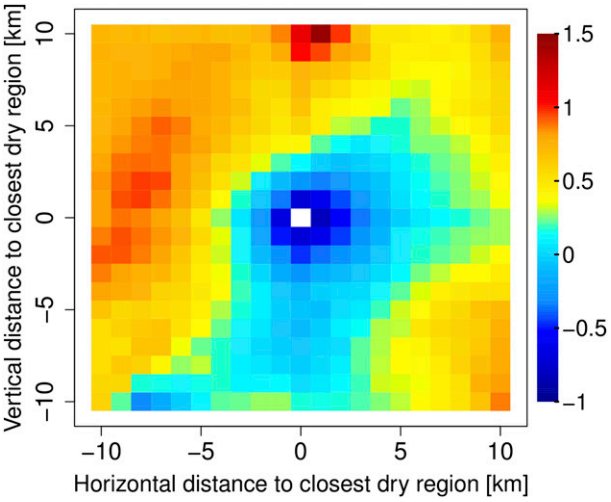

FIG. 6. Estimated anisotropic dry drift for the rain-rate map shown in Fig. 3. One can see that the dry drift is stronger (i.e., it increases faster) in the northwest direction than in the south, east, and northeast directions.

system. They might therefore exhibit a strongly anisotropic dry drift. Orographic enhancement of precipitation may also lead to anisotropy. In most of the analyzed cases, however, the isotropic dry drift adequately described the general trend in the data.

4. Other types of dry drifts

a. Temporal dry drift

In the following, we briefly describe the equivalent of the dry drift for intermittent rainfall time series. The approach is essentially similar to the two-dimensional dry drifts, except that the spatial coordinates $\mathbf{x} \in \mathbb{R}^2$ are replaced by a single time coordinate $t \in \mathbb{R}$. The reparameterization of the rainfall intensity process is not based on the Euclidean distance but on the time τ to the closest dry period:

$$\tau: \mathbb{R} \mapsto \mathbb{R}^+, \tag{17}$$

$$\tau(t) = \min_{u \in \Omega} \{|t - u|\}, \tag{18}$$

$$\Omega = \{u \in \mathbb{R} \,|\, I_R(u) = 0\}, \quad \text{and} \tag{19}$$

$$m_{\tilde{R}}(t) = f[\tau(t)]. \tag{20}$$

An example of a temporal dry drift is shown in Fig. 7. One can see that spatial and temporal dry drifts have very similar shapes and intensities. This is not a coincidence and can be explained using Taylor's hypothesis of frozen turbulence (e.g., Taylor 1938; Gupta and Waymire 1990; Fabry 1996). Consider a space–time rainfall

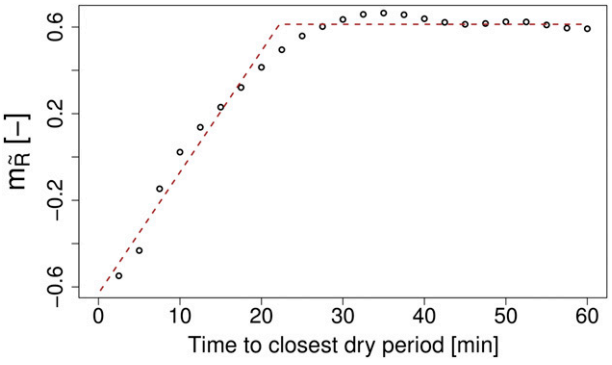

FIG. 7. Estimated isotropic temporal dry drift for the domain shown in Fig. 3 and the rain event on 1 Aug 2012, between 1600 and 2359 UTC. The dashed red line represents the fitted piecewise linear dry drift model. The class width is 2.5 min.

field $R(\mathbf{x}, t)$ with constant storm movement velocity vector $\mathbf{v} \in \mathbb{R}^2$. If $R(\mathbf{x}, t)$ is slowly evolving in time, any time series $R(\mathbf{x}_0, t)$ (at a particular location $\mathbf{x}_0$) can be approximately converted into a one-dimensional range profile in the direction of $\mathbf{v}$:

$$R(\mathbf{x}_0, t) \approx R(\mathbf{x}_0 - \mathbf{v}dt, t - dt) \quad \forall \quad t \in \mathbb{R}, \quad \forall \quad dt \in \mathbb{R}. \tag{21}$$

On average, this is a reasonable approximation for dt values up to ±20–30 min (Li et al. 2009). For larger values of dt, the relation progressively breaks down because of changes in the storm movement and because of the temporal evolution of R. Obviously, the same approximation applies (and is even better) for the rainfall occurrence process I_R:

$$I_R(\mathbf{x}_0, t) \approx I_R(\mathbf{x}_0 - \mathbf{v}dt, t - dt) \quad \forall \quad t \in \mathbb{R}, \quad \forall \quad dt \in \mathbb{R}. \tag{22}$$

One of the consequences of this relationship in space and time is that the distance $d(\mathbf{x}_0)$ (along $\mathbf{v}$) from $\mathbf{x}_0$ at time t to the closest dry region will be approximately equal to the time $\tau(t - dt)$ from $t - dt$ to the closest time period at location $\mathbf{x}_0 - \mathbf{v}dt$. This is what creates the link between the dry drift in time and the dry drift in space (at least along $\mathbf{v}$). Note that by comparing the distance of influence d_M of the spatial dry drift with the time of influence τ_M of the temporal dry drift, it is possible to estimate the average storm movement velocity. In the present case (i.e., Fig. 7), $d_M = 7.5$ km and $\tau_M = 20$ min, and the average storm movement velocity is approximately 22.5 km h^{-1} (which is consistent with the "true" value derived from the radar rain-rate maps). Note also that if there is no advection, the temporal and spatial dry drifts can still be linked through a so-called time regularization parameter (e.g., Lepioufle et al. 2012).

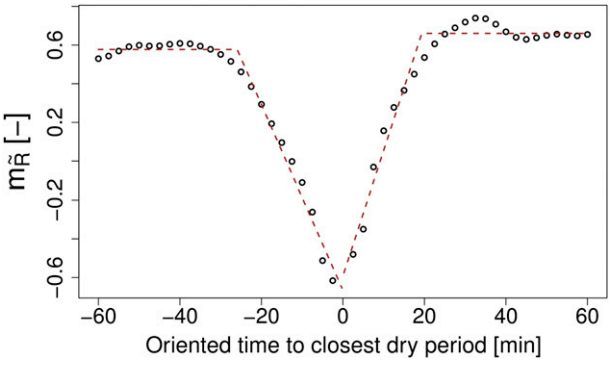

FIG. 8. Estimated asymmetric temporal dry drift for the domain shown in Fig. 3 and the rain event on 1 Aug 2012, between 1600 and 2359 UTC. The dashed red line represents the fitted piecewise linear dry drift models. Negative time lags mean that the closest dry period lies in the past. Positive time lags correspond to situations where the closest time period is ahead. The class width is 2.5 min.

Similarly to isotropic and anisotropic spatial dry drifts, we distinguish between symmetric and asymmetric temporal dry drifts. In the symmetric case, the dry drift solely depends on the time τ to the closest dry period. In the asymmetric case, the dry drift depends both on the time and on the relative position (before/after) of the closest dry period:

$$m_{\tilde{R}}(t) = g[\Delta(t)], \tag{23}$$

where $g\colon \mathbb{R} \mapsto \mathbb{R}$ and $\Delta(t) \in \mathbb{R}$ represents the (oriented) time from t to the closest dry period. For a visual illustration of this concept, see Fig. 8. In this figure, we can see that the temporal dry drift for negative values of Δ (i.e., when the closest dry period lies in the past) is slightly weaker ($m_1 = -0.05$ and $M = 0.58$) than the temporal dry drift for positive values of Δ ($m_1 = 0.07$ and $M = 0.66$). The difference is, however, very small, and it is reasonable to assume a symmetric model as shown in Fig. 7.

b. *Space–time dry drift*

The strong relation between the spatial and the temporal dry drift mentioned in the previous section can also be used to formulate more general space–time dry drifts. In this case, the dry drift $f\colon \mathbb{R}^2 \mapsto \mathbb{R}$ becomes a function of the distance to the closest dry region and of the time to the closest dry period, as shown in Fig. 9. The simplest possible space–time dry drift model corresponding to this case is obtained by taking the minimum between the isotropic dry drift in space and the symmetric dry drift in time:

$$m_{\tilde{R}}(d,\tau) = \min\left[m_0 + m_1 \cdot \min\left\{d, \frac{d_M}{\tau_M}\tau\right\}, M\right], \tag{24}$$

where m_0, m_1, and M are given in Eq. (8). This is, however, not the only possible way of modeling a space–time

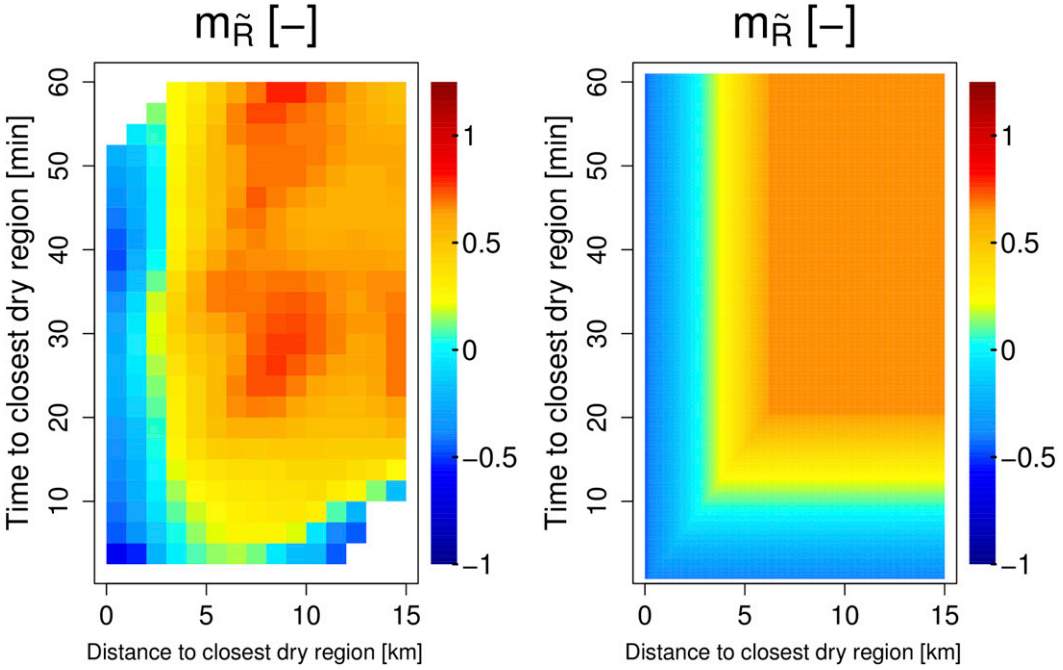

FIG. 9. (left) Estimated isotropic space–time dry drift corresponding to the event shown in Fig. 3 and (right) corresponding fitted dry drift model given in Eq. (24).

dry drift. Further extensions and generalizations (e.g., including spatial anisotropy and/or temporal asymmetry) can be considered but will not be detailed here.

c. Dry drifts for DSD-related quantities

The DSD is a very general and detailed statistical description of the microstructure of rainfall. Its purpose is to efficiently summarize (using probability theory and statistics) the huge amount of information about the drops contained in a given volume of air. In its traditional definition, the DSD describes the expected number of drops with equivolume spherical drop diameters between D and $D + dD$ per unit volume (m^3) of air:

$$N(D, \mathbf{x}, t) = N_t(\mathbf{x}, t) \cdot \nu(D, \mathbf{x}, t), \tag{25}$$

where $N_t(\mathbf{x}, t)$ (m^{-3}) represents the drop concentration at location $\mathbf{x}$ and time t and $\nu(D, \mathbf{x}, t)$ (mm^{-1}) is a probability density function that describes the size distribution of the drop diameters at location $\mathbf{x}$ and time t. Knowledge of the DSD is very useful in practical applications because it allows one to derive (through numerical integration) most quantities of interest related to rainfall. The average drop diameter, the kinetic energy, the rain rate, and the liquid water content are all weighted moments of the DSD. Assuming a drop size–shape relationship (e.g., Andsager et al. 1999; Beard et al. 2010), the DSD also allows one to derive most quantities of interest in remote sensing like the radar reflectivity, the specific attenuation, and the differential phase shift.

Like the rain rate, the DSD is influenced by surrounding dry regions and should not be considered independent from the rainfall occurrence process I_R (e.g., Schleiss et al. 2012, 635–636). In this section, we show that it is possible to extend the concept of dry drifts (explained previously for rain-rate values) to the DSD and to all other quantities expressed as weighted moments of the DSD. The major difference compared with the rain rate is that the DSD can be affected by two different types of dry drifts: 1) a dry drift on the drop concentration N_t and 2) a dry drift on the size distribution ν. Most of the time, both the drop concentration and the average drop size decrease when approaching a dry region. The rates and magnitudes of these two drifts are, however, very different. Typically, the dry drift on N_t is much stronger than the dry drift on ν. The fact that N_t and ν can have different dry drifts has important consequences and means, for example, that DSD-related quantities like the average drop diameter, the rain rate, and the radar reflectivity (which all depend differently on the DSD) will be affected by different dry drifts. The mass weighted mean drop diameter, for example, solely depends on the size distribution ν and will be completely insensitive to dry drifts in N_t. The rain rate on the other hand, depends both on N_t and on ν and will be affected by a combination of both dry drifts. The radar reflectivity is also affected by both dry drifts but, because it is a higher-order moment of the average drop diameter than the rain rate, it will be more sensitive to dry drifts in ν. This can have several important consequences and means, in particular that the Z–R relationship changes with respect to d (see section 5 for more details).

To illustrate the concept of dry drift for DSD-related quantities, the authors analyzed DSD time series collected by a network of disdrometers deployed in the region of Ardèche, France (see section 2b). The network is neither big enough nor dense enough to analyze the spatial dry drifts of DSD-related quantities, but it can be used to study the dry drifts in the time domain. In this case, the large number of instruments is only used to check the consistency of the results and to verify that they are not dependent on the location of the sensor. An example of a measured DSD time series is shown in the top panel of Fig. 10. The collected DSD spectra were used to derive the drop concentration N_t (m^{-3}), the mass-weighted mean drop diameter D_m (mm) (which is independent of N_t and will be used as a proxy for the size distribution ν), and the rain rate R ($mm\,h^{-1}$):

$$N_t = \int_{D_{\min}}^{D_{\max}} N(D, t)\, dD, \tag{26}$$

$$D_m(t) = \frac{\int_{D_{\min}}^{D_{\max}} N(D, t) D^4\, dD}{\int_{D_{\min}}^{D_{\max}} N(D, t) D^3\, dD}, \quad \text{and} \tag{27}$$

$$R(t) = \frac{6\pi}{10^4} \int_{D_{\min}}^{D_{\max}} D^3 v(D) N(D, t)\, dD, \tag{28}$$

where $v(D)$ ($m\,s^{-1}$) represents the average terminal fall speed of a drop with equivolume spherical diameter D (mm) (e.g., Beard 1976).

The temporal dry drifts affecting $\tilde{N}_t = \log_{10}(N_t)$, D_m, and $\tilde{R}$ are shown in Fig. 11. Note that because there were relatively few data, the dry drifts shown in this figure were estimated using a 3-min class width instead of the original 30-s resolution. The average value of $\tilde{N}$ varies from 2.2 at $\tau = 30$ s to 2.9 at $\tau = 80$ min and stays relatively constant afterward. The average value of the mass-weighted mean drop diameter D_m varies from 0.9 mm at $\tau = 30$ s to 1.5 mm at $\tau = 105$ min. The drift affecting N_t is therefore about twice as strong (in linear space) as the dry drift affecting D_m. The "time of

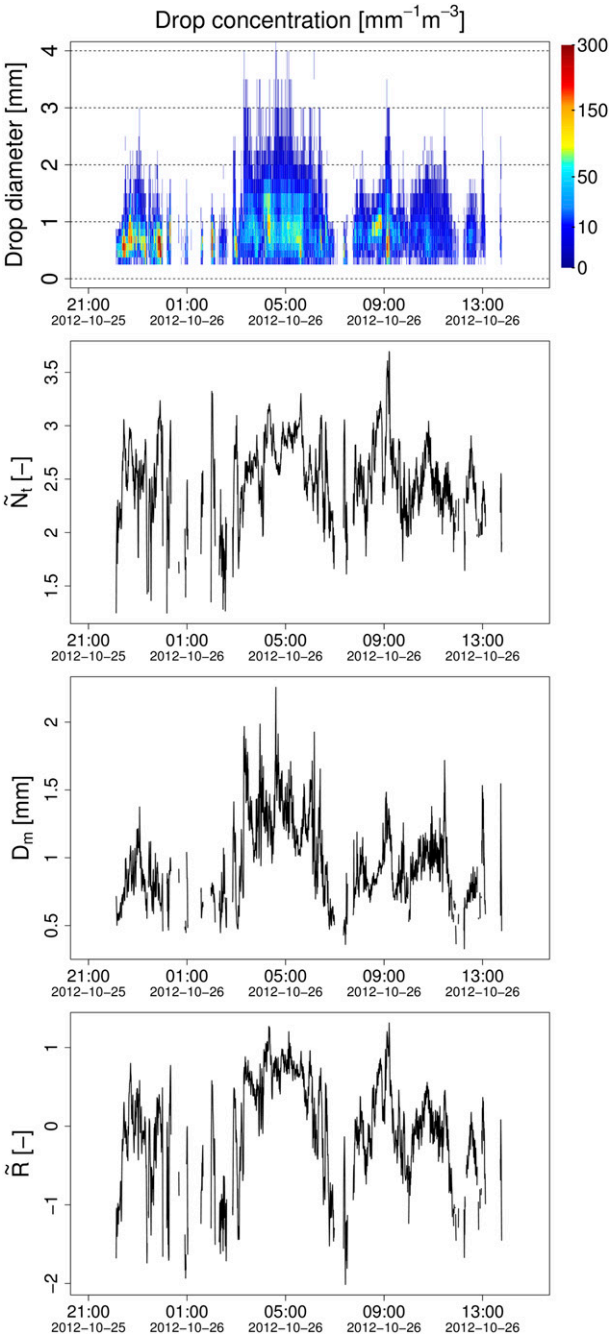

FIG. 10. (top to bottom) Measured DSD time series for a rain event on the 25–26 October 2012 and corresponding values of $\tilde{N}_t = \log_{10}(N_t)$, D_m, and $\tilde{R} = \log_{10}(R)$. The temporal resolution is 30 s.

influence'' τ_M is, however, slightly larger for D_m than for $\tilde{N}_t$. Because it depends both on N_t and on D_m, the dry drift affecting $\tilde{R}$ is a combination between the dry drift of $\tilde{N}_t$ and of D_m. Note also that the time of influence is slightly larger than in Fig. 7.

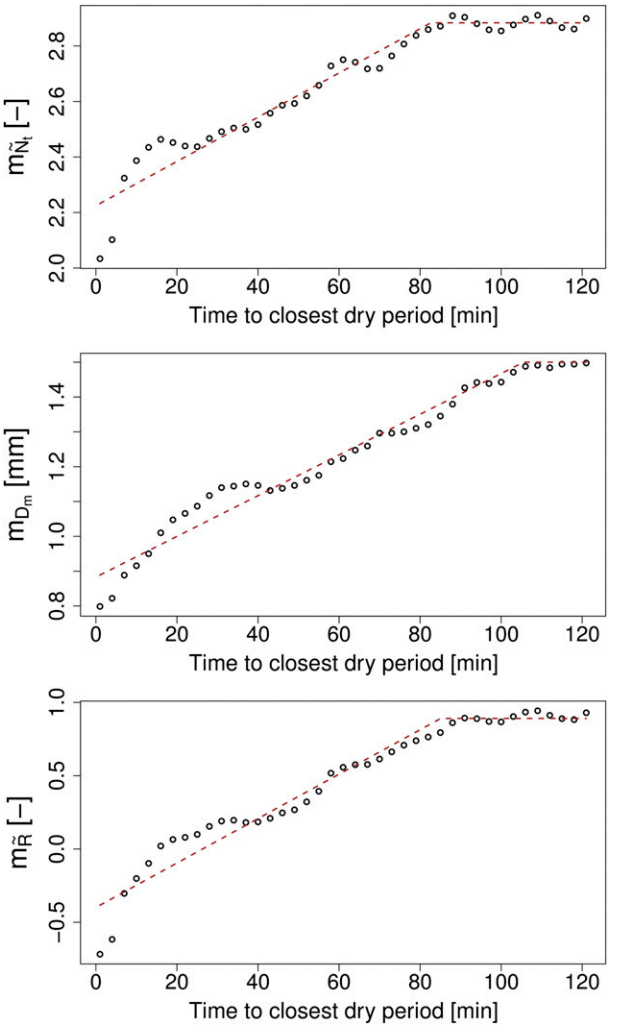

FIG. 11. Estimated (temporal) dry drifts of $\tilde{N}_t = \log_{10}(N_t)$, D_m, and $\tilde{R} = \log_{10}(R)$ for the rain event shown in Fig. 10. The dashed red lines represent the fitted dry drift models. The class width is 3 min.

5. Importance of dry drifts

In this section, we present some examples and applications that highlight the importance of dry drifts in rainfall analysis, modeling, and remote sensing.

a. Importance for structural analysis

One of the most important consequences of the dry drift is the fact that the expected rain rate varies (nonlinearly) in space and time. The rainfall intensity process R (or equivalently, $\tilde{R}$) is therefore neither second-order nor intrinsically stationary. If the drift is strong enough, it might affect the sample variogram of R (respectively, $\tilde{R}$). This can lead to a serious misinterpretation of the spatial and temporal correlation structure and the variability of the rainfall intensity field (Starks and Fang

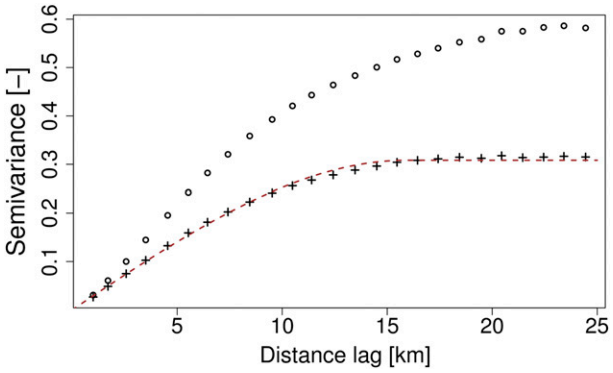

FIG. 12. Isotropic sample variograms of log-transformed rain rates (for the radar rain-rate map shown in Fig. 3) before (dots) and after (crosses) removal of the dry drift. The dashed red line represents a fitted spherical variogram model.

1982). In some particular cases, the sample variogram may exhibit unexpected features, like a strong decrease at larger distance lags. These decreases cannot be explained using the traditional geostatistical framework, but they can be understood easily within the dry drift formalism. The decrease of the semivariance at larger distance lags simply results from the action of the dry drift and a particular geometrical disposition of dry areas within the domain.

A better and mathematically more correct approach in the presence of a nonlinear drift is to 1) start by estimating the dry drift $f(d)$, 2) remove it, and 3) compute the sample variogram of the detrended process $R^\star$ (see section 3b). The spatial structure and variability of the rainfall field is then described through the combination of a deterministic part (i.e., the dry drift) and the variogram of the detrended rain-rate process. To illustrate the difference, the authors computed the sample variograms corresponding to the radar rain-rate map shown in Fig. 3, before and after removal of the dry drift. The two obtained sample variograms are shown in Fig. 12. One can see that the sample variogram of the detrended rain-rate process has a well-defined sill and range. It is easier to interpret and to model than the sample variogram computed from the initial rain-rate map. By comparing the two variograms, one can also notice that the dry drift explains about 50% of the total spatial variability of the considered rain-rate field (in log space). In other words, both the shape and the variability of the rainfall field are strongly determined by the dry drift. For more details about this subject, see section 5b.

In the following, a new way of modeling an intermittent rainfall field that extends the approach proposed by Barancourt et al. (1992) is proposed. In this new model, three different components are necessary to describe the spatial structure and variability of an intermittent rain-rate field:

1) the spatial distribution and structure of the rainfall occurrence process, described by the percentage p_0 of dry regions and the variogram $\gamma_{I_R}(\mathbf{h})$ of I_R (which can be assumed second-order stationary);
2) a deterministic rainfall trend defined by the dry drift function $f(d)$ and the location of the dry areas in the considered domain; and
3) the spatial structure of the rain-rate field after removal of the dry drift, described by the variogram $\gamma_{\tilde{R}^\star}(\mathbf{h})$ of $R^\star$.

b. *Explained variability*

In the following, we propose an objective way of quantifying the importance of the dry drift function in structural analysis of rain-rate fields. The method consists of comparing the sample variance of the log-transformed rain-rate field $\tilde{R}$ with the sample variance of the new rain-rate field $R^\star$ obtained after removal of the dry drift:

$$\rho = 1 - (\hat{\sigma}^2_{R^\star}/\hat{\sigma}^2_{\tilde{R}}), \tag{29}$$

where $\hat{\sigma}^2_{\tilde{R}}$ and $\hat{\sigma}^2_{R^\star}$ are the sample variances of $\tilde{R}$ and $R^\star$. Because it involves the ratio of these two quantities, ρ measures the percentage of total variability that is explained by the dry drift. If $\rho = 1$, the dry drift "explains" the entire variability of the rain-rate field. If $\rho = 0$, the dry drift explains nothing. Systematic analysis of 14 stratiform and 14 convective events shows that, on average, the isotropic two-dimensional dry drift model explains 31.7% of the total variability of stratiform events and 37.4% of the total variability of convective events (at 5-min temporal resolution and for log-transformed rain-rate values). These percentages even go up to 45% for stratiform and 52% for convective events if an anisotropic dry drift is considered (see section 3d). These are nonnegligible values and mean that the dry drift plays an important role in structuring intermittent rainfall fields. For some individual time steps with large numbers of dry regions, the isotropic dry drift explained more than 80% of the total variability. Interestingly, the amount of explained variability grows with decreasing temporal resolution. For 1-h aggregated radar rain-rate maps (with a spatial resolution of $1 \times 1\,\text{km}^2$), the average explained variability for the isotropic dry drift was 59% for stratiform events and 69% for convective events. This can be explained by the fact that rain-rate fields at lower temporal resolutions are smoother and therefore better described by the dry drift. However, because the number of dry regions decreases

with lower temporal resolutions (i.e., there are fewer and fewer dry areas), it also becomes more difficult to reliably estimate the dry drift over small domains.

c. Probability distribution of average rain rate

Another important and interesting aspect of the dry drift is the fact that the shape and size of a rainy area, together with the dry drift function $f(d)$, fully determine the probability distribution function (pdf) of the average rain rate $m_{\tilde{R}}$. For some basic geometrical shapes, it is even possible to obtain analytical expressions for the pdf. To illustrate this, let us consider two simple cases: 1) a continuous rainy period of total duration equal to T and 2) a circular rain cell with diameter D. For more generality, we assume that $T/2 > \tau_M$ and $D/2 > d_M$, where τ_M and d_M represent the maximum time (respectively distance) of influence of the dry drift.

1) Case 1: Continuous rainy period of duration T

For a continuous rainy period of duration T, the probability distribution of τ (i.e., the time to the closest dry period) is given by

$$P[\tau \le u] = \begin{cases} 0 & \text{if} \quad u \le 0 \\ \dfrac{2}{T} & \text{if} \quad 0 < u < \dfrac{T}{2}. \\ 1 & \text{if} \quad u \ge \dfrac{T}{2} \end{cases} \tag{30}$$

Combining this equation with the expression for a symmetric piecewise linear dry drift leads to

$$P[m_{\tilde{R}} \le m] = \begin{cases} 0 & \text{if} \quad m < m_0 \\ \dfrac{2}{T}\left(\dfrac{m - m_0}{m_1}\right) & \text{if} \quad m_0 < m < M\,. \\ 1 & \text{if} \quad m \ge M \end{cases} \tag{31}$$

The average value of $m_{\tilde{R}}$ for a continuous rainy period of duration T is therefore given by

$$\overline{m}_{\tilde{R}} = \frac{\tau_M}{T}(M + m_0) + (T - 2\tau_M)M = M - \frac{\tau_M}{T}(M - m_0). \tag{32}$$

2) Case 2: Circular rain cell of diameter D

For a circular rain cell of diameter D, the pdf of d (i.e., the distance to the closest dry region) is given by

$$P[d \le u] = \begin{cases} 0 & \text{if} \quad u \le 0 \\ 1 - \dfrac{\left(\dfrac{D}{2} - u\right)^2}{\left(\dfrac{D}{2}\right)^2} & \text{if} \quad 0 < u < \dfrac{D}{2}. \\ 1 & \text{if} \quad u \ge \dfrac{D}{2} \end{cases} \tag{33}$$

Simplifying this expression and combining it with the equation for an isotropic piecewise linear dry drift leads to

$$P[m_{\tilde{R}} \le m] = \begin{cases} 0 & \text{if} \quad m < m_0 \\ 1 - \left[1 - \dfrac{2(m - m_0)}{m_1 D}\right]^2 & \text{if} \quad m_0 < m < M\,. \\ 1 & \text{if} \quad m \ge M \end{cases} \tag{34}$$

Furthermore, the mean value of $m_{\tilde{R}}$ inside the rain cell is given by

$$\overline{m}_{\tilde{R}} = M\frac{(D - 2d_M)^2}{D^2} + \frac{4}{D^2}\int_0^{d_M} (m_0 + m_1 u)(D - 2u)\, du, \tag{35}$$

which, after integration and simplification, leads to

$$\overline{m}_{\tilde{R}} = M - 4\frac{d_M}{D}(M - m_0) + 4\left(\frac{d_M}{D}\right)^2\left(M - m_0 + m_1\frac{D}{2} - \frac{2m_1 d_M}{3}\right). \tag{36}$$

Such simple calculations nicely illustrate how the dry drift can be used to predict average areal/temporal rain rates depending on the shape and the size of a given rain cell/period.

d. Variability of the Z–R relationship

It is well known that weather radars do not directly measure the rain rate R (which is the quantity of interest in most applications) but the reflectivity Z ($\mathrm{mm^6\,m^{-3}}$), which depends on the DSD. Transformations that allow one to estimate R given Z are called Z–R relationships. The most common Z–R relationship is a simple power law (Marshall and Palmer 1948):

$$Z = aR^b, \tag{37}$$

where a and b are two parameters that depend on the time, the location, and the type of rainfall. In fact, the

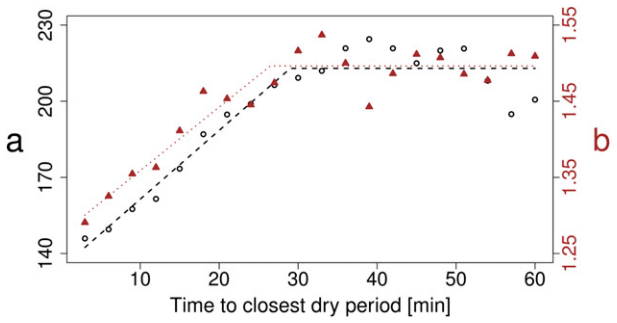

FIG. 13. Climatological estimates of the prefactor a (black circles) and exponent b (red triangles) in the Z–R relationship as a function of the time to the closest dry period. The parameters a and b have been estimated using the DSD time series collected by the seven disdrometers in Ardèche, France. The black (red) dotted line represents the dry drift for the a (b) parameter.

optimal values of a and b strongly depend on the drop size distribution (which is usually unknown in practical applications). A common solution to this problem is to rely on climatological relationships and to estimate a and b using large datasets of different rain events that are supposed to be representative of the local climatology. For example, Marshall et al. (1955) suggested

$$Z = 200R^{1.6}. \tag{38}$$

The problem with climatological Z–R relationships is that they only represent the average relationship between Z and R. As a result, rain rates derived using this technique can be strongly biased. In addition to this well-known problem, it is worth mentioning that because R and Z are affected differently by the dry drifts in the DSD (see section 4c), the average Z–R relationship also changes with the distance d to the closest dry region:

$$Z = a(d)R^{b(d)}. \tag{39}$$

Unfortunately, this effect is very difficult to observe and to quantify in two-dimensional rain-rate fields: it requires large and dense sets of spatial DSD measurements that are not available so far. Its existence can, however, be illustrated using simple DSD time series. Figure 13 shows the temporal dry drift that affects the Z–R relationship as a function of the time τ to the closest dry period. One can see that the values of a and b (obtained by fitting the Z–R relationship for each class of τ) clearly increase with τ until they reach a maximum of $a = 210$ and $b = 1.50$ at $\tau = 30$ min. In other words, one needs to wait about 30 min after the start of an event until the Z–R relationship can be considered "stable." This corresponds, assuming an average storm movement velocity of 20 km h^{-1}, to approximately 10 km in space. This is a nonnegligible distance and means that it might be necessary to reconsider the way the Z–R relationship is applied close to dry regions.

e. *Rainfall simulation*

Stochastic simulation is a very powerful tool to quantify the uncertainties associated with spatial and temporal variability of rainfall. Simulated rain-rate fields are free from any measurement noise and errors and can therefore be used to investigate various issues related to rainfall scaling and error propagation in hydrologic and climatic models. Simulation also offers the advantage of reproducibility, that is, the fact that many similar and statistically homogeneous alternative realizations of a given rain event can be generated. This is a clear advantage over direct observations where each event is unique and can only be observed once. The goal of this section is not to provide an exhaustive review of the many different rainfall simulators and rainfall simulation techniques that have been proposed in the literature, but to highlight the importance of dry drifts for rainfall simulation.

Figure 14 shows two simulated intermittent rain-rate fields, without (top panel) and with (bottom panel) dry drift. Both fields have the same intermittency, average rain rate, and standard deviation. They were generated using the following procedure: first, the sequential indicator algorithm was used to generate an indicator field with a spherical variogram (nugget = 0, sill = 0.24, and range = 24 km). The outcome of this simulation was then used to define the dry and the rainy areas in the domain. Second, a Gaussian field with zero mean and a standard deviation of 1.3 was generated using sequential Gaussian simulation (for the rain locations only) and another spherical variogram (nugget = 0, sill = 1.7, and range = 12 km). In the first case (top panel), no dry drift was applied. A simple exponential transform was applied to obtain the final lognormal rain-rate distribution. In the second case (bottom panel), an additional dry drift was added before back transformation.

One can see that in the first simulation (without dry drift), the occurrence and intensity process are independent. The average rain rate is not influenced by surrounding dry regions. Transitions between dry and rainy regions can be arbitrarily steep. In the second field (with dry drift), the average rain rate depends on the location of the dry areas. On average, there is a smoother transition between dry and rainy regions. Both the spatial structure and the rain-rate distribution inside the rainy areas are believed to be more realistic.

6. Summary and perspectives

In this article, we revisited an important aspect of the nonstationary nature of intermittent rainfall fields, that

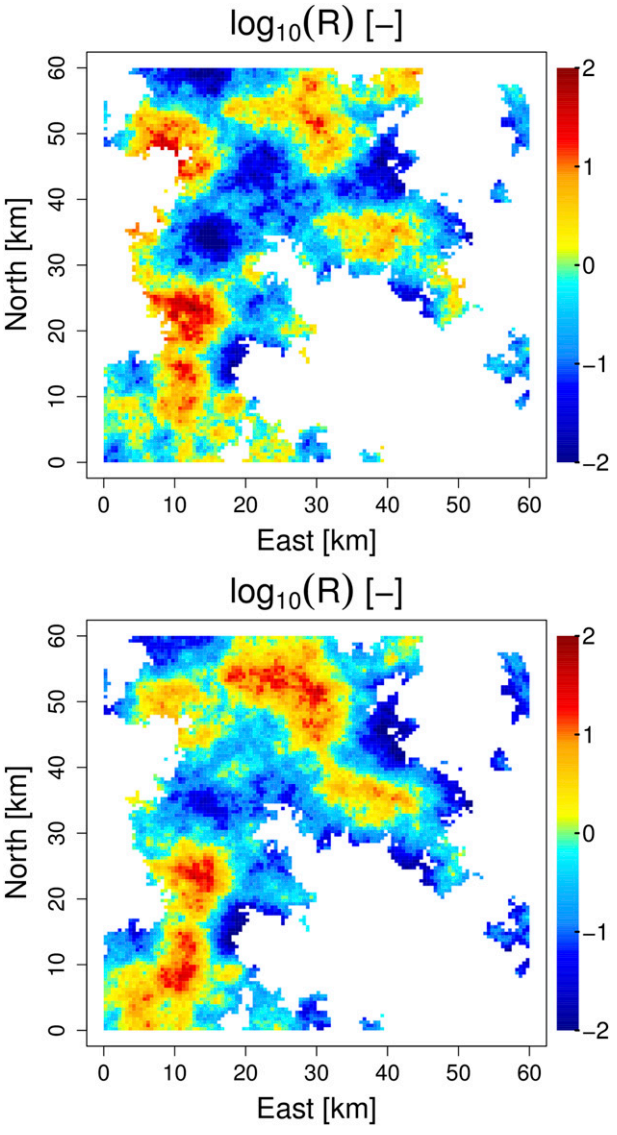

FIG. 14. Example of a simulated rain-rate field (top) without and (bottom) with dry drift.

is, the fact that the average rain rate varies with the distance/time to the closest surrounding dry region/period. We called this fundamental link between rainfall intensity and occurrence the dry drift. The existence, shape, and characteristics of dry drifts in space and time were illustrated using radar and disdrometer data. Because of the large skewness and the heteroscedasticity of rain rates, the authors proposed to estimate and model dry drifts in the log space rather than in the linear parameter space.

The analysis of 14 stratiform and 14 convective events showed that dry drifts constitute a very general feature and can be found both in stratiform and convective rain events (with different parameter values). On average, the isotropic two-dimensional dry drift model explained about 35% of the total variability (in the log space and at 5-min temporal resolution) of an intermittent rainfall field and significantly affected its sample variogram.

Several interesting questions and issues were raised in this paper. Some of them have profound implications and will have to be investigated more thoroughly in future studies. The first issue concerns the existence and shape of the dry drift for different rainfall types and climatologies. It was shown that a piecewise linear dry drift model (corresponding to an exponential increase/decrease in linear space) provides a fair fit for both stratiform and convective rain events in Switzerland. The linear model is based on empirical observations rather than physical considerations. To what extent this model is transferable to other countries and climatologies still needs to be investigated. The fact that similar dry drift functions (although in the temporal domain) were observed for data collected in the south of France, however, increases our confidence in the linear dry drift model and strengthens our belief that dry drifts are not specific to radar data collected in Switzerland.

The second issue concerns the estimation of the dry drift from sample rain-rate fields. A critical point in this procedure appears to be the ability to estimate the distance $d(\mathbf{x})$ from $\mathbf{x}$ to the closest dry region in the domain. This is rather straightforward with radar data but more problematic using rain gauge networks (Braud et al. 1994). In rain gauge networks, the distance to the closest dry region cannot be determined accurately (depending on the density of the network). Hence, Eq. (11) cannot be used to estimate the dry drift. This is a clear limitation in practical applications where the dry drift needs to be estimated and parameterized from rain gauge measurements.

The third issue that requires more detailed investigations is the question of scale and the dependency of dry drifts to spatial and temporal resolution. Some preliminary results presented in section 5b show that the variability explained by dry drifts increases at lower spatial and temporal resolutions. This can be explained by the "smoothing effect," that is, the fact that the average variability of rainfall decreases with scale (both in space and in time). However, the exact magnitude and rate of this effect still need to be quantified.

The fourth issue that needs to be investigated is the question of whether the detrended rain-rate field $R^{\star}$ (after removal of the dry drift) can be considered second-order stationary or not. Clearly, the dry drift is not the only source of nonstationarity in rainfall. Other drifts, caused, for example, by orographic effects, coast

lines, or seasonal/daily variations in precipitation patterns, may also play an important role. Finding an appropriate mathematical framework that allows one to take into account (and combine) all these different sources of nonstationarity at different scales is a difficult problem that still needs to be investigated.

Finally, another important finding of this paper is the fact that the (rain)drop size distribution (DSD) is affected by two different dry drifts: one for the drop concentration and another for the size distribution. The fact that these two drifts are not equal and greatly vary from one event to another is very interesting. The authors believe that it may be possible to use these differential drifts in the DSD to retrieve some important information about the different microphysical processes at work (e.g., collisional growth or breakup). Future work will mainly focus on these aspects and on their consequences for remote sensing applications.

Acknowledgments. The authors acknowledge the financial support by the CCES project TRAMM2 (Grant 3022) and thank MeteoSwiss for providing the radar data used in this study. The disdrometer data were obtained from the HyMeX program, sponsored by Grants MISTRALS/HyMeX, ANR-2011-BS56-027 FLOODSCALE project, and EPFL-LTE.

REFERENCES

Andsager, K., K. V. Beard, and N. F. Laird, 1999: Laboratory measurements of axis ratios for large rain drops. *J. Atmos. Sci.,* **56,** 2673–2683, doi:10.1175/1520-0469(1999)056<2673:LMOARF>2.0.CO;2.

Barancourt, C., J.-D. Creutin, and J. Rivoirard, 1992: A method for delineating and estimating rainfall fields. *Water Resour. Res.,* **28,** 1133–1144, doi:10.1029/91WR02896.

Beard, K. V., 1976: Terminal velocity and shape of cloud and precipitation drops aloft. *J. Atmos. Sci.,* **33,** 851–864, doi:10.1175/1520-0469(1976)033<0851:TVASOC>2.0.CO;2.

——, V. N. Bringi, and M. Thurai, 2010: A new understanding of raindrop shape. *Atmos. Res.,* **97,** 396–415, doi:10.1016/j.atmosres.2010.02.001.

Berrocal, V. J., A. E. Raftery, and T. Gneiting, 2008: Probabilistic quantitative precipitation field forecasting using a two-stage spatial model. *Adv. Atmos. Sci.,* **2,** 1170–1193, doi:10.1214/08-AOAS203.

Braud, I., P. Crochet, and J. D. Creutin, 1994: A method for estimating mean areal rainfall using moving trend functions of the intensities. *J. Appl. Meteor.,* **33,** 1551–1561, doi:10.1175/1520-0450(1994)033<1551:AMFEMA>2.0.CO;2.

de Montera, L., L. Barthès, C. Mallet, and P. Golé, 2009: The effect of rain–no rain intermittency on the estimation of the universal multifractals model parameters. *J. Hydrometeor.,* **10,** 493–506, doi:10.1175/2008JHM1040.1.

De Oliveira, V., 2004: A simple model for spatial rainfall fields. *Stochastic Environ. Res. Risk Assess.,* **18,** 131–140, doi:10.1007/s00477-003-0146-4.

Emmanuel, I., H. Andrieu, E. Leblois, and B. Flahaut, 2012: Temporal and spatial variability of rainfall at the urban hydrological scale. *J. Hydrol.,* **430–431,** 162–172, doi:10.1016/j.jhydrol.2012.02.013.

Fabry, F., 1996: On the determination of scale ranges for precipitation fields. *J. Geophys. Res.,* **101,** 12 819–12 826, doi:10.1029/96JD00718.

Germann, U., G. Galli, M. Boscacci, and M. Bolliger, 2006: Radar precipitation measurement in a mountainous region. *Quart. J. Roy. Meteor. Soc.,* **132,** 1669–1692, doi:10.1256/qj.05.190.

Gires, A., I. Tchiguirinskaia, D. Schertzer, and S. Lovejoy, 2013: Development and analysis of a simple model to represent the zero rainfall in a universal multifractal framework. *Nonlinear Processes Geophys.,* **20,** 343–356, doi:10.5194/npg-20-343-2013.

Gupta, V. K., and E. Waymire, 1990: Multiscaling properties of spatial rainfall and river flow distributions. *J. Geophys. Res.,* **95,** 1999–2009, doi:10.1029/JD095iD03p01999.

Jaffrain, J., A. Studzinski, and A. Berne, 2011: A network of disdrometers to quantify the small-scale variability of the raindrop size distribution. *Water Resour. Res.,* **47,** W00H06, doi:10.1029/2010WR009872.

Journel, A. G., 1980: The lognormal approach to predicting local distributions of selective mining unit grades. *Math. Geol.,* **12,** 285–303, doi:10.1007/BF01029417.

Kumar, P., and E. Foufoula-Georgiou, 1993: A multicomponent decomposition of spatial rainfall fields: 1. Segregation of large- and small-scale features using wavelet transforms. *Water Resour. Res.,* **29,** 2515–2532, doi:10.1029/93WR00548.

Kundu, P. K., and R. K. Siddani, 2011: Scale dependence of spatiotemporal intermittence of rain. *Water Resour. Res.,* **47,** W08522, doi:10.1029/2010WR010070.

Lepioufle, J.-M., E. Leblois, and J.-D. Creutin, 2012: Variography of rainfall accumulation in presence of advection. *J. Hydrol.,* **464–465,** 494–504, doi:10.1016/j.jhydrol.2012.07.041.

Li, B., A. Murthi, K. Bowman, G. North, M. Genton, and M. Sherman, 2009: Statistical tests of Taylor's hypothesis: An application to precipitation fields. *J. Hydrometeor.,* **10,** 254–265, doi:10.1175/2008JHM1009.1.

Löffler-Mang, M., and J. Joss, 2000: An optical disdrometer for measuring size and velocity of hydrometeors. *J. Atmos. Oceanic Technol.,* **17,** 130–139, doi:10.1175/1520-0426(2000)017<0130:AODFMS>2.0.CO;2.

Mandapaka, P. V., W. F. Krajewski, R. Mantilla, and V. K. Gupta, 2009: Dissecting the effect of rainfall variability on the statistical structure of peak flows. *Adv. Water Resour.,* **32,** 1508–1525, doi:10.1016/j.advwatres.2009.07.005.

Marshall, J. S., and W. M. Palmer, 1948: The distribution of raindrops with size. *J. Meteor.,* **5,** 165–166, doi:10.1175/1520-0469(1948)005<0165:TDORWS>2.0.CO;2.

——, W. Hitschfeld, and K. L. S. Gunn, 1955: Advances in radar weather. *Advances in Geophysics,* Vol. 2, Academic Press, 1–56, doi:10.1016/S0065-2687(08)60310-6.

Olsson, J., 1998: Evaluation of a scaling cascade model for temporal rainfall disaggregation. *Hydrol. Earth Syst. Sci.,* **2,** 19–30, doi:10.5194/hess-2-19-1998.

Over, T. M., and V. K. Gupta, 1994: Statistical analysis of mesoscale rainfall: Dependence of a random cascade generator on large-scale forcing. *J. Appl. Meteor.,* **33,** 1526–1542, doi:10.1175/1520-0450(1994)033<1526:SAOMRD>2.0.CO;2.

Porporato, A., and I. Rodriguez-Iturbe, 2004: Soil water balance and ecosystem response to climate change. *Amer. Nat.,* **164,** 625–632, doi:10.1086/424970.

Schleiss, M., J. Jaffrain, and A. Berne, 2011: Statistical analysis of rainfall intermittency at small spatial and temporal scales. *Geophys. Res. Lett.,* **38,** L18403, doi:10.1029/2011GL049000.

——, ——, and ——, 2012: Stochastic simulation of intermittent DSD fields in time. *J. Hydrometeor.,* **13,** 621–637, doi:10.1175/JHM-D-11-018.1.

Schmitt, F., S. Vannitsem, and A. Barbosa, 1998: Modeling of rainfall time series using two-state renewal processes and multifractals. *J. Geophys. Res.,* **103,** 23 181–23 193, doi:10.1029/98JD02071.

Starks, T. H., and J. H. Fang, 1982: The effect of drift on the experimental semivariogram. *Math. Geol.,* **14,** 309–319, doi:10.1007/BF01032592.

Syed, K. H., D. C. Goodrich, D. E. Myers, and S. Sorooshian, 2003: Spatial characteristics of thunderstorm rainfall fields and their relation to runoff. *J. Hydrol.,* **271,** 1–21, doi:10.1016/S0022-1694(02)00311-6.

Taylor, G. I., 1938: The spectrum of turbulence. *Proc. Roy. Soc. London,* **164,** 476–490, doi:10.1098/rspa.1938.0032.